Molecular Mechanisms of Bone ^{18}F-NaF Deposition

Johannes Czernin, Nagichettiar Satyamurthy, and Christiaan Schiepers

Ahmanson Biological Imaging Division, Department of Molecular and Medical Pharmacology, David Geffen School of Medicine at the University of California, Los Angeles

There is renewed interest in ^{18}F-NaF bone imaging with PET or PET/CT. The current brief discussion focuses on the molecular mechanisms of ^{18}F-NaF deposition in bone and presents model-based approaches to quantifying bone perfusion and metabolism in the context of preclinical and clinical applications of bone imaging with PET.

Key Words: ^{18}F-NaF; bone fluoride deposition; PET/CT

J Nucl Med 2010; 51:1826–1829
DOI: 10.2967/jnumed.110.077933

There is renewed interest in imaging malignant, metabolic, degenerative, traumatic, and inflammatory bone diseases using ^{18}F-NaF, a bone imaging probe that was initially introduced by Blau et al. in 1962 (*1*). ^{18}F-NaF became the standard method for bone scintigraphy in the 1960s but was largely replaced by ^{99}Tc-labeled diphosphonate compounds in the 1970s (*2*) because of their better physical characteristics for imaging with conventional γ-cameras.

The reemergence of ^{18}F-NaF bone imaging was ignited by the introduction of PET (*3*) and PET/CT (*4*) (Fig. 1), which permits assessment of bone diseases with a higher accuracy than planar imaging or SPECT; the availability of electronic generators allowing for the widespread use of ^{18}F-NaF (*5*); and the well-documented shortage of ^{99}Mo/^{99}Tc generators leading to limited availability of ^{99}Tc.

Because clinical studies using PET and PET/CT bone imaging approaches have been reviewed extensively (*6–9*), the current discussion focuses on the molecular mechanisms of ^{18}F-NaF deposition in bone. After a brief description of the radiosynthesis, the kinetics and biodistribution of ^{18}F-NaF in vivo are described. Furthermore, model-based approaches to quantifying bone perfusion and metabolism are presented in the context of preclinical and clinical applications of bone imaging with PET.

PREPARATION OF ^{18}F-NaF

^{18}F-fluoride is produced by 11-MeV proton irradiation of ^{18}O-water in a tantalum target body (*10*) using a cyclotron. The irradiated aqueous solution containing ^{18}F-fluoride is diluted with sterile water (5 mL) and passed through a cation exchange (H^+ form) cartridge. The eluent from the cation exchange cartridge is passed through an anion exchange (HCO_3^- form) cartridge to trap the ^{18}F-fluoride. The anion exchange cartridge is then flushed with 10 mL of sterile water, and the ^{18}F fluoride is then eluted with 10 mL of sterile normal saline and is passed through a sterile filter into a sterile multidose vial. The quality control tests for the ^{18}F-NaF are conducted according to the method of the U.S. Pharmacopeia (*11*).

KINETICS OF ^{18}F-NaF

The rate-limiting step of ^{18}F-NaF bone uptake is blood flow (*12*), and almost all ^{18}F-NaF delivered is retained by bone after a single pass of blood (*13*). The initial ^{18}F-NaF distribution therefore represents blood flow that varies among different bones (*14*). Uptake of tracer by the bone marrow is negligible (*15*). Around 30% of the injected ^{18}F-NaF is present in erythrocytes, but this fact does not impede ion exchange in bone because ^{18}F-NaF is freely diffusible across membranes (*16*). ^{18}F-NaF is rapidly cleared from plasma and excreted by the kidneys. One hour after injection, only 10% of ^{18}F-NaF remains in plasma, and the 5-h integrated plasma concentration was only 1.1%–2.6% of the dose per liter. The 5-h cumulative urine excretion was 7.4%–24.8% in 8 patients (*17*).

For bone deposition, ^{18}F-ions need to "pass from plasma through the extracellular fluid space into the shell of bound water surrounding each crystal, onto the crystal surface and in the interior of the crystal," as described by Blau et al. (*12*). After chemisorption onto hydroxyapatite, ^{18}F exchanges rapidly for OH on the surface of the hydroxyapatite matrix ($Ca_{10}(PO_4)_6OH_2$) to form fluoroapatite ($Ca_{10}(PO_4)_6F_2$) (*18*). The incorporation of ^{18}F into bone matrix as fluoroapatite is slow (days to weeks) (*12*).

Bone surface encompasses 300 m^2/g of bone tissue for a total of 3×10^6 m^2 for the whole body (*19*). ^{18}F-NaF uptake and retention in bone depends on the area of the "exposed" bone surface, which is larger in a variety of benign and malignant bone disorders. The relationship between osteoblastic and osteoclastic activity determines the incorporation of ^{18}F-NaF into the bone matrix (*20*). Negligible plasma protein binding, rapid blood and renal clearance (*21*), and high bone uptake early after injection result in high target-to-background ratios, which in turn permit whole-body imaging as early as 45–60 min after tracer injection.

TRACER KINETIC MODELS

Quantitative bone imaging is potentially important because several metabolic bone diseases are subtle at onset, diffuse in nature, and difficult to detect with other techniques, including blood- or urine-derived biomarkers or other imaging techniques

Received Jun. 30, 2010; revision accepted Aug. 20, 2010.
For correspondence or reprints contact: Johannes Czernin, UCLA, Ahmanson Biological Imaging Division, 10833 Le Conte Avenue, Room AR-125 CHS, Los Angeles, CA 90095-1782.
E-mail: jczernin@mednet.ucla.edu
Guest Editor: Barry Siegel, Mallinckrodt Institute of Radiology

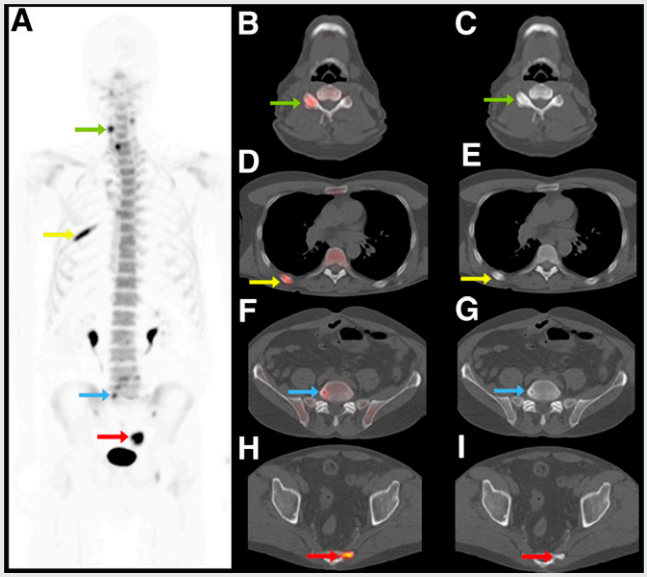

FIGURE 1. Maximum-intensity-projection PET image (A) and selected axial PET/CT (B, D, F, H) and CT (C, E, G, I) images of ^{18}F-NaF PET/CT scan of 63-y-old man with prostate cancer. Increased ^{18}F-NaF uptake can be seen in benign changes of right cervical facet joint (green arrow in A, B, and C), healing rib fracture (yellow arrow in A, D, and E), benign lumbar vertebral bone cyst (blue arrow in A, F, and G), and blastic metastasis in sacrum (red arrow in A, H, and I). Additional value of CT to characterize focally increased tracer uptake is evident.

(*22*). For instance, measurements of bone density are of unknown prognostic value for fracture risk assessments and unproven for monitoring disease during treatment (*23*). Quantitative measurements of bone blood flow and metabolism can be derived from dynamic PET with ^{18}F-NaF and appropriate tracer kinetic models. Such models can provide quantitative measurements in patients with a variety of bone diseases and might greatly aid drug response assessments.

The model that best describes fluoride incorporation into bone is a simple 3-compartment model (*18*) consisting of a vascular, an extravascular, and a bone compartment. The model describes regional rather than whole-body pharmacokinetics (*24,25*) (Fig. 2) and is similar to the standard in vivo model for ^{18}F-FDG (*26*). This and other models have been described previously (*27,28*).

ANIMAL EXPERIMENTAL STUDIES

PET has been used to measure bone blood flow (*29*), first-pass bone extraction fraction (*30*), whole-body biodistribution (*21,31*), tracer kinetics (*24,25*), and the pharmacokinetics (*17*) of ^{18}F-NaF. These and other studies were reviewed extensively by Blake et al. (*8*).

The normal kinetics and biodistribution of ^{18}F-NaF have also been exploited to study physiologic processes. For instance, assessing renal function is of critical importance in preclinical drug development. Traditionally, this requires blood and urine sampling, which is difficult in small animals. Because renal fluoride clearance is related to the glomerular filtration rate, the pharmacokinetics of ^{18}F-NaF were used to assess renal function in rats (*32*). The ^{18}F-NaF–based measurements correlated well

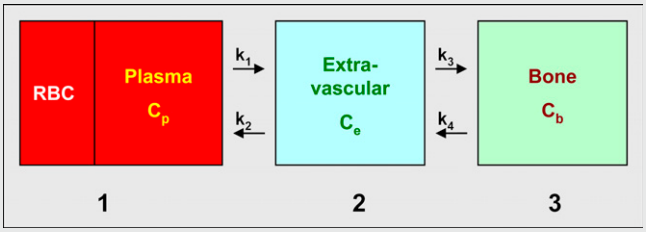

FIGURE 2. ^{18}F-NaF kinetic model with 3 compartments: vascular (1), extravascular (2), and bone (3). Plasma clearance of ^{18}F-NaF is measured in left ventricle or aorta with PET scanner or from arterial blood draw; k_1–k_4 are rate constants; k_1 and k_2 represent forward and reverse transport from plasma, and k_3 and k_4 represent uptake and release from bone. If extraction fraction equals 1, then k_1 represents local bone blood flow. Influx rate $K_i = k_1 \cdot k_3 \cdot (k_2 + k_3)^{-1}$ is related to Ca^{2+} influx and bone apposition rate and, presumably, represents bone remodeling rate. Ki is determined by both bone blood flow and bone turnover. Therefore, measurements have to be interpreted in context of each individual study. Respective concentrations of fluoride are denoted as C_p (in plasma), C_e (in extravascular space), and C_b (in bone compartment). RBC = red blood cells

with traditional measurements of renal function derived from imaging (^{99}Tc-mercaptoacetyltriglycine) and from serum markers, suggesting that this quantitative method could be used for measuring renal function preclinically and clinically. However, given the existence of other accurate tests, this application is less likely to be adopted clinically in the near future.

Several animal experimental studies have used quantitative approaches to describe alterations in bone blood flow and metabolism in a variety of diseases.

Trauma

Dworkin et al. (*21*) examined the biodistribution and pharmacokinetics of ^{18}F-NaF in fractured and nonfractured bone in dogs at variable times after a surgically induced tibia fracture. They observed a time-dependent accumulation of ^{18}F-NaF without increased tracer uptake at the fracture site 3 h after injury but increasing uptake from 3 wk to 3 mo, suggesting that bone healing and therapeutic interventions can be monitored in animal experimental models.

To investigate the impact of chronic stress and fatigue, the ulna of rats was exposed to cyclic compressions at various subfracture levels (*33*). This resulted in increased bone vascularity as early as 1 d after stress, which was followed by periosteal bone formation at day 3. ^{18}F-NaF uptake correlated with these histopathologic changes, which in turn reflected the severity of induced stress. Tracer uptake returned to normal at 24 d after stress, suggesting that this assay could be used to monitor stress responses of bone.

Metabolic Bone Diseases

Novel agents targeting bone loss are being developed (*34*). The potential of PET-derived quantitative measurements of treatment-induced changes in bone flow and metabolism in drug development and clinical trials is obvious.

The equilibrium between bone formation and resorption is altered in many metabolic bone disorders, including primary and secondary hyperparathyroidism, renal osteodystrophy, osteoporo-

sis, and others. Histomorphometric measurements can be used to evaluate bone formation invasively. PET was used to demonstrate in mini pigs that quantitative measurements of bone blood flow and metabolism can be derived from dynamic ^{18}F-NaF imaging (*20*) and that these noninvasive measurements correlate well with invasive assessments of bone turnover.

Murine Tumor Models

^{18}F-NaF PET bone imaging protocols have been optimized in mice. The coefficient of variation from 4 consecutive measurements as an index of reproducibility of ^{18}F-NaF bone uptake was less than 15% when bone counts per pixel per minute were normalized to a region of interest encompassing the whole skeleton (*35*). The excellent reproducibility supports the use of ^{18}F-NaF small-animal PET to study a variety of bone diseases.

Small-animal PET or PET/CT has been used to image relevant models of metastatic prostate cancer and to monitor natural disease progression. For instance, the formation of osteolytic, osteoblastic, and mixed bone metastases from prostate cancer was studied with small-animal ^{18}F-NaF and ^{18}F-FDG PET/CT scans, radiographs, and histology or histomorphometry (*36*). ^{18}F-NaF and ^{18}F-FDG PET/CT accurately identified osteoblastic lesions and their progression (Fig. 3). Mixed blastic–lytic lesions were well visualized only with ^{18}F-FDG, whereas ^{18}F-NaF uptake was low or absent. In pure lytic lesions, ^{18}F-FDG uptake increased over time. In contrast, ^{18}F-NaF uptake was initially high but decreased to background levels after 6 wk, suggesting early increases in tumor vascularization resulting in flow-dependent accumulation of the probe.

Another group injected human Ewing sarcoma cells subcutaneously or intravenously into immune-deficient mice (*37*). Small-animal PET with ^{18}F-FDG and ^{18}F-NaF was then used to search for soft-tissue, lung, and bone metastases. Only intravenous tumor cell injection reproduced the human metastatic pattern (lung, bone, and soft tissue). In contrast to the study by Hsu et al. (*36*), Ewing sarcoma bone lesions exhibited decreased ^{18}F-NaF uptake relative to normal bone. This difference is most likely explained by the use of a different tumor model and the different timing of PET scans after tumor cell injection.

Thus, relevant animal models of primary and metastatic bone lesions that mimic the biologic behavior of these tumors in humans were generated. These models can be used to evaluate novel bone imaging agents or to monitor the effects of therapeutic interventions on the course of primary or secondary bone malignancies.

QUANTITATIVE HUMAN STUDIES

The long-term precision and reproducibility of quantitative bone metabolism measurements with ^{18}F-NaF PET was established by Frost et al. (*38*) in patients with osteopenia or osteoporosis. All underwent PET scans of the lumbar spine at baseline and after 6 mo. Measurement precision and reproducibility were compared with biomarkers of bone formation. The coefficient of variation was comparable among PET-based measurements and nonimaging biomarkers. In general, the precision of PET-based measurements ranged from 10% to 15%.

Hawkins et al. (*18*) measured an average influx rate of 0.036 ± 0.006 mL/min/mL in healthy bones (*18*). Schiepers et al. (*28*) reported a blood flow to lumbar vertebrae of 0.058 mL/min/mL and influx of 0.022 mL/min/mL for osteoporosis. For Paget disease, the flow rate was 0.205 mL/min/mL (or 4 times higher than flow to normal bone) and the influx was 0.114 mL/min/mL. Using the same model (Fig. 2), Cook et al. (*27*) also found an almost 4-fold increase in Paget-affected bones.

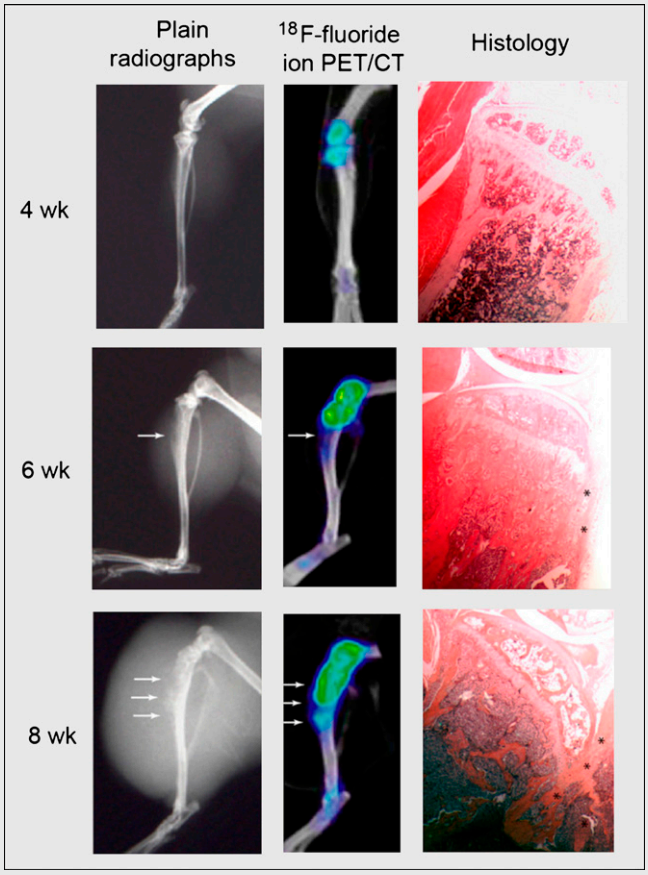

FIGURE 3. Radiographs (left), ^{18}F-NaF PET/CT scans (middle), and photomicrographs of histologic specimen (right). PET/CT images reveal osteoblastic lesion earlier (4 wk) than radiography (arrows denote bone lesions). Increasing ^{18}F-NaF uptake over time corresponds to increased bone formation seen on histology (asterisks). (Reprinted from (*36*).)

Messa et al. (*39*) measured bone flow and fluoride influx in patients with renal osteodystrophy and primary hyperparathyroidism and found significantly increased influx rates that decreased by 30%–40% after parathyroidectomy and medical therapy. Excellent correlations between influx rates and serum alkaline phosphatase and parathyroid hormone levels, as well as histomorphometric indices of bone formation rate, were reported.

The blood flow to the femoral head was estimated by Schiepers et al. (*40*) in 5 patients with unilateral hip trauma. A flow ratio of greater than 2 between the abnormal and normal femoral head was necessary for a successful outcome with conservative treatment. A minimum flow of 0.04 mL/min/mL was measured in 1 patient whose affected femoral head healed conservatively.

Using the model shown in Figure 2 (*18,28*), Frost et al. studied bone flow and turnover in women with treated and untreated metabolic bone disease (*14*). Bone perfusion was highly variable between the lumbar spine and the humerus, an observation that

was not attainable by biomarkers of global bone turnover or by biopsy.

CONCLUSION

^{18}F-NaF PET or PET/CT is a well-established and validated qualitative and quantitative imaging tool. Because PET is fundamentally superior to conventional planar imaging and SPECT, and because of the favorable pharmacokinetics of ^{18}F-NaF allowing for early imaging after tracer injection, PET or PET/CT bone imaging will eventually replace conventional ^{99}Tc-based γ-camera techniques in the clinic. Moreover, therapeutic interventions targeting metabolic, degenerative, traumatic, and neoplastic bone diseases will be assessed for their effectiveness in preclinical research and clinical practice.

REFERENCES

1. Blau M, Nagler W, Bender M. Fluorine-18: a new isotope for bone scanning. *J Nucl Med.* 1962;3:332–334.
2. Subramanian G, McAfee J. A new complex of ^{99m}Tc for skeletal imaging. *Radiology.* 1971;99:192–196.
3. Phelps ME, Hoffman EJ, Mullani NA, Ter-Pogossian MM. Application of annihilation coincidence detection to transaxial reconstruction tomography. *J Nucl Med.* 1975;16:210–224.
4. Townsend DW. Dual-modality imaging: combining anatomy and function. *J Nucl Med.* 2008;49:938–955.
5. Satyamurthy N, Phelps ME, Barrio JR. Electronic generators for the production of positron-emitter labeled radiopharmaceuticals: where would PET be without them? *Clin Positron Imaging.* 1999;2:233–253.
6. Langsteger W, Heinisch M, Fogelman I. The role of fluorodeoxyglucose, ^{18}F-dihydroxyphenylalanine, ^{18}F-choline, and ^{18}F-fluoride in bone imaging with emphasis on prostate and breast. *Semin Nucl Med.* 2006;36:73–92.
7. Fogelman I, Cook G, Israel O, Van der Wall H. Positron emission tomography and bone metastases. *Semin Nucl Med.* 2005;35:135–142.
8. Blake GM, Park-Holohan S, Cook G, Fogelman I. Quantitative studies of bone with the use of ^{18}F-fluoride and ^{99m}Tc-methylene diphosphonate. *Semin Nucl Med.* 2001;31:28–49.
9. Grant FD, Fahey FH, Packard AB, Davis RT, Alavi A, Treves ST. Skeletal PET with ^{18}F-fluoride: applying new technology to an old tracer. *J Nucl Med.* 2008;49:68–78.
10. Satyamurthy N, Amarasekera B, Alvord C, Barrio J, Phelps M. Tantalum [^{18}O] water target for the production of [^{18}F] fluoride with high reactivity for the preparation of 2-deoxy-2-[^{18}F] fluoro-D-glucose. *Mol Imaging Biol.* 2002;4:65–70.
11. Sodium fluoride F 18 injection. Rockville, MD: U.S. Pharmacopeia; 2009. USP 32-NF 27.
12. Blau M, Ganatra R, Bender M. 18 F-fluoride for bone imaging. *Semin Nucl Med.* 1972;2:31–37.
13. Wootton R, Dore C. The single-passage extraction of ^{18}F in rabbit bone. *Clin Phys Physiol Meas.* 1976;7:333–343.
14. Frost ML, Blake GM, Cook GJ, Marsden PK, Fogelman I. Differences in regional bone perfusion and turnover between lumbar spine and distal humerus: ^{18}F-fluoride PET study of treatment-naive and treated postmenopausal women. *Bone.* 2009; 45:942–948.
15. Reeve J, Arlot M, Wootton R, et al. Skeletal blood flow, iliac histomorphometry, and strontium kinetics in osteoporosis: a relationship between blood flow and corrected apposition rate. *J Clin Endocrinol Metab.* 1988;66:1124–1131.
16. Carlson CH, Armstrong WD, Singer L. Distribution, migration and binding of whole blood fluoride evaluated with radiofluoride. *Am J Physiol.* 1960;199:187–189.
17. Weber DA, Greenberg EJ, Dimich A, et al. Kinetics of radionuclides used for bone studies. *J Nucl Med.* 1969;10:8–17.
18. Hawkins RA, Choi Y, Huang SC, et al. Evaluation of the skeletal kinetics of fluorine-18-fluoride ion with PET. *J Nucl Med.* 1992;33:633–642.
19. Newman W, Newman M. *The Chemical Dynamics of Bone Mineral*. Chicago, IL: University of Chicago Press; 1958.
20. Piert M, Zittel TT, Becker GA, et al. Assessment of porcine bone metabolism by dynamic [^{18}F]fluoride ion PET: correlation with bone histomorphometry. *J Nucl Med.* 2001;42:1091–1100.
21. Dworkin H, Moon N, Lessard R, LaFleur P. A study of the metabolism of fluorine-18 in dogs and its suitability for bone scanning. *J Nucl Med.* 1966; 7:510–520.
22. Green AD, Colon-Emeric CS, Bastian L, Drake MT, Lyles KW. Does this woman have osteoporosis? *JAMA.* 2004;292:2890–2900.
23. Cummings SR, Bates D, Black DM. Clinical use of bone densitometry: scientific review. *JAMA.* 2002;288:1889–1897.
24. Charkes ND, Brookes M, Makler PT Jr. Studies of skeletal tracer kinetics: II. Evaluation of a five-compartment model of [^{18}F]fluoride kinetics in rats. *J Nucl Med.* 1979;20:1150–1157.
25. Charkes ND, Makler PT Jr, Philips C. Studies of skeletal tracer kinetics. I. Digital-computer solution of a five-compartment model of [^{18}F] fluoride kinetics in humans. *J Nucl Med.* 1978;19:1301–1309.
26. Phelps ME, Huang SC, Hoffman EJ, Selin C, Sokoloff L, Kuhl DE. Tomographic measurement of local cerebral glucose metabolic rate in humans with (F-18)2-fluoro-2-deoxy-D-glucose: validation of method. *Ann Neurol.* 1979;6:371–388.
27. Cook GJ, Blake GM, Marsden PK, Cronin B, Fogelman I. Quantification of skeletal kinetic indices in Paget's disease using dynamic ^{18}F-fluoride positron emission tomography. *J Bone Miner Res.* 2002;17:854–859.
28. Schiepers C, Nuyts J, Bormans G, et al. Fluoride kinetics of the axial skeleton measured in vivo with fluorine-18-fluoride PET. *J Nucl Med.* 1997;38:1970–1976.
29. Vandyke D, Anger H, Yano Y, Bozzini C. Bone blood flow shown with F18 and the positron camera. *Am J Physiol.* 1965;209:65–70.
30. Wootton R. The single-passage extraction of ^{18}F in rabbit bone. *Clin Sci Mol Med.* 1974;47:73–77.
31. Ackerhalt RE, Blau M, Bakshi S, Sondel JA. A comparative study of three ^{99m}Tc-labeled phosphorus compounds and ^{18}F-fluoride for skeletal imaging. *J Nucl Med.* 1974;15:1153–1157.
32. Schnöckel U, Reuter S, Stegger L, et al. Dynamic ^{18}F-fluoride small animal PET to noninvasively assess renal function in rats. *Eur J Nucl Med Mol Imaging.* 2008;35:2267–2274.
33. Silva MJ, Uthgenannt BA, Rutlin JR, Wohl GR, Lewis JS, Welch MJ. In vivo skeletal imaging of ^{18}F-fluoride with positron emission tomography reveals damage- and time-dependent responses to fatigue loading in the rat ulna. *Bone.* 2006;39:229–236.
34. Deal C. Future therapeutic targets in osteoporosis. *Curr Opin Rheumatol.* 2009;21:380–385.
35. Berger F, Lee Y, Loening A, et al. Whole-body skeletal imaging in mice utilizing microPET: optimization of reproducibility and applications in animal models of bone disease. *Eur J Nucl Med Mol Imaging.* 2002;29:1225–1236.
36. Hsu WK, Virk M, Feeley B, Stout D, Chatziioannou A, Lieberman J. Characterization of osteolytic, osteoblastic, and mixed lesions in a prostate cancer mouse model using ^{18}F-FDG and ^{18}F-fluoride PET/CT. *J Nucl Med.* 2008;49:414–421.
37. Franzius C, Hotfilder M, Poremba C, et al. Successful high-resolution animal positron emission tomography of human Ewing tumours and their metastases in a murine xenograft model. *Eur J Nucl Med Mol Imaging.* 2006;33:1432–1441.
38. Frost ML, Blake GM, Park-Holohan SJ, et al. Long-term precision of ^{18}F-fluoride PET skeletal kinetic studies in the assessment of bone metabolism. *J Nucl Med.* 2008;49:700–707.
39. Messa C, Goodman WG, Hoh CK, et al. Bone metabolic activity measured with positron emission tomography and [^{18}F]fluoride ion in renal osteodystrophy: correlation with bone histomorphometry. *J Clin Endocrinol Metab.* 1993;77: 949–955.
40. Schiepers C, Broos P, Miserez M, Bormans G, De Roo M. Measurement of skeletal flow with positron emission tomography and F-18-fluoride in femoral head osteonecrosis. *Arch Orthop Trauma Surg.* 1998;118:131–135.